Electrochemical Synthesis for Flowerlike and Fusiform Christmas-Tree-like Cerium Hexacyanoferrate(II)

Liang-Dong Feng,[†,‡] Miao-Miao Gu,[†] Yan-Li Yang,[†] Guo-Xi Liang,[†] Jian-Rong Zhang,[†] and Jun-Jie Zhu*[,†,§]

Key Laboratory of Analytical Chemistry for Life Science (MOE), School of Chemistry and Chemical Engineering, Nanjing University, Nanjing 210093, P. R. China, Key Laboratory for Attapulgite Science and Applied Technology of Jiangsu Province, Department of Chemical Engineering, Huaiyin Institute of Technology, Huaian 223003, P. R. China, and State Key Laboratory of Bioelectronics (Chien-Shiung Wu Laboratory), Southeast University, Nanjing 210096, P. R. China

Received: February 1, 2009; Revised Manuscript Received: March 19, 2009

A facile electrochemical approach was developed for the controllable synthesis of cerium hexacyanoferrate(II) (CeHCF(II)) flowerlike and fusiform Christmas-tree-like microparticles. The composition, morphology, and structure of the as-prepared CeHCF(II) products were characterized by the techniques such as powder X-ray diffraction (XRD), infrared spectroscopy (IR), thermogravimetry (TG), differential scanning calorimetry (DSC), X-ray photoelectron spectroscopy (XPS), energy-dispersive X-ray spectroscopy (EDS), and scanning electron microscopy (SEM). The formula of the prepared CeHCF(II) could be assigned to be $KCe[Fe(CN)_6]\cdot 4H_2O$. It was observed that the size and morphology of the CeHCF(II) microparticles were altered by electrodepositing potential and time, the molar ratio of $Ce(NO_3)_3$ and $K_3[Fe(CN)_6]$, and the acidity of electrolyte. To the best of our knowledge, this morphologies of CeHCF(II) have not been reported before. The as-prepared CeHCF(II) microparticles showed good ultraviolet luminescent properties and high luminescent intensity.

Introduction

In the past decades, based on the effective intermolecular energy transfers from the coordinated ligands to the luminescent central of lanthanide ions, rare earth compounds have been studied intensively for their unique optical properties and high luminescence quantum efficiency.[1] Their versatile luminescent properties have inspired vigorous research activities and been applied in a wide range of fields, such as optical materials,[2] bioassays,[3] and sensor systems.[4] The 4f electrons of lanthanide ions are well shielded from the neighboring ions. The shielding effect results in discrete and well-defined energy level schemes, as well as weak coupling between the electronic and vibrational wave functions. The f−f emissions of lanthanide ions lead to long lifetime luminescent properties. However, the progress with regard to new luminescent materials is chiefly focused on short emission wavelengths at present, which is useful in lithography, imaging, and optical data recording.[5] The Ce^{3+} and Sm^{2+} ions exhibit a 5d−4f emission with a large absorption in the ultraviolet (UV) region and a short luminescence lifetime due to allowed electric dipole transitions. The 5d−4f transition of trivalent cerium ions results in a broad-band emission in the UV to visible range. Since electrons in the 5d state take part in the formation of chemical bonds (in the excited state), the position of the excitation and emission bands depends strongly on the host lattice, i.e., the crystal structure and composition.[6] Compared to other trivalent lanthanide ions, the notable luminescent property of Ce^{3+} ion is its short luminescence lifetime and high light output, and it makes Ce^{3+}-containing solids promising materials in several applications.[7] But unfortunately, the light output of luminescent materials is often affected by the concentration aggregation and the material's size and morphology. When the concentration of the luminescent central increases, the ion distance becomes comparable to the critical distance, at which the radiative decay probability equals the energy transfer rate, leading to nonradiative processes and resulting in concentration quenching.[6a,8] The luminescent efficiency of nanoparticles is usually lower than that of the corresponding bulk material, which is due to the energy quenching in energy-transfer processes originating from surface trapping states in the nanostructures. In recent years, much progress has been made to significantly increase the luminescent efficiency of nanosized materials by suppressing energy-loss processes in the energy-transfer processes.[9−12] Therefore, it is important to control the luminescence material size, morphology, and distance of luminescent centrals.

As potential advanced materials, self-assembled microstructure and nanostructures with specific morphology and novel chemical and physical properties have attracted great attention.[13,14] Much progress has been made in the preparation, and the luminescent properties of different morphology and size of cerium compounds, such as CeP,[15,16] $CePO_4$,[17−21] $CeVO_5$,[22−25] CeF_3,[26−28] and Ce^{3+} ion doping materials were observed.[29−37] As for the metal cyanides, the interesting photoluminescence properties of $M[Ag(CN)_2]_3$ (M = La, Tb, Eu, Dy) have been studied extensively,[38] but there is only a few studies involving the preparation and the properties of Prussian blue (PB, ferric hexacyanoferrate(II), $Fe_4[Fe(CN)_6]_3\cdot xH_2O$) and its analogues.[39] Until now, to the best of our knowledge, no reports were involved with cerium hexacyanoferrates(II) (CeHCF(II)).

Herein, we describe a facile electrochemical preparation of microsized flowerlike and fusiform Christmas-tree-like CeHCF(II), and the highly efficient ultraviolet luminescent properties were observed. The structure and composition of the as-prepared

* To whom correspondence should be addressed. E-mail: jjzhu@nju.edu.cn. Tel./Fax: +86-25-8359-4976.
[†] Nanjing University.
[‡] Huaiyin Institute of Technology.
[§] Southeast University.

10.1021/jp900925p CCC: $40.75
Published on Web 04/22/2009

CeHCF(II) were characterized with X-ray powder diffraction (XRD), infrared spectruoscopy (IR), thermogravimetry (TG), differential scanning calorimetry (DSC), energy-dispersive X-ray spectroscopy (EDS), and X-ray photoelectron spectroscopy (XPS) techniques. The morphology and size of the final products were investigated by scanning electron microscopy (SEM). It was found to be a fast, convenient route for the preparation of different shapes and sizes of CeHCF(II) microparticles. On the coordinated CN^- ligands, CeHCF(II) showed good ultraviolet luminescent properties, and it had high light output attributed to the proper distance of Ce^{3+} ions in CeHCF(II) and the moderate particle size and shape.

Experimental Section

Materials and Characterizations. Analytical grade cerium nitrate ($Ce(NO_3)_3$), potassium hexacyanoferrate(III) ($K_3[Fe(CN)_6]$), potassium nitrate (KNO_3), and nitric acid (HNO_3) were purchased from Shanghai Chemical Reagent Co. All reagents were used without further purification, and distilled water was used throughout.

Powder XRD measurement was performed on a Shimadzu XD-3A X-ray diffractometer at a scanning rate of 4°/min in the 2θ range from 10 to 80°, with graphite-monochromatized Cu Kα radiation ($\lambda = 0.154\,06$ nm) and nickel filter. IR spectroscopy was carried out on a Bruker Ifs66 Fourier transform infrared (FTIR) spectrometer (Bruker Co.) with KBr (FTIR grade) pellet in the single-beam mode over the range of 400−4000 cm^{-1} at room temperature. The TG and DSC curves were recorded in a Shimadzu TGA-50 instrument. The XPS patterns were recorded on an ESCALAB MK II X-ray photoelectron spectrometer by using nonmonochromatized Al Kα X-ray as the excitation source and choosing C1s (284.6 eV) as the reference line. The SEM images and EDS spectra were carried out on a S-3000 N (Hitachi, Japan) scanning electron microscope with EX-250 (Horiba, Japan) operating at 20 kV.

Electrochemical experiments were carried out on a CHI 660C electrochemical workstation (Chenhua, Shanghai, China) at room temperature. A traditional three-electrode configuration was used with an indium tin oxide (ITO) slide as the working electrode. A platinum wire and a saturated calomel electrode (SCE) served as counter electrode and reference electrode, respectively. All potentials given below were relative to the SCE.

Ultraviolet visible (UV−vis) absorption spectra were measured on a UV−vis Recording Spectrophotometer (UV-2401 PC, Shimadzu). Photoluminescence (PL) spectra were recorded with a fluorescence spectrophotometer (FL, Hitachi F-4500). Dispersions of the resulting products in water were measured in standard quartz cuvettes at room temperature.

Preparation of CeHCF(II). The flowerlike and fusiform Christmas-tree-like CeHCF(II) microparticles were synthesized by amperometric method. In a typical procedure, the ITO electrode was immersed into the mixture containing 5.0 mM $Ce(NO_3)_3$, 5.0 mM K_3 $[Fe(CN)_6]$, and 0.1 M KNO_3, and the potential was kept at a certain value for given times. Then, the ITO electrode was gently washed with doubly distilled water to remove the adsorbed salts. The ITO slide with deposited CeHCF(II) was dried in a desiccator for SEM and EDS measurements. For IR, TG, XPS, XRD, UV−vis, and PL measurements, the electrodeposited CeHCF(II) was scraped from the ITO slide by a stainless steel knife.

Results and Discussion

The powered XRD pattern of the CeHCF(II) deposited at −0.2 V for 500 s in 0.1 M KNO_3 is shown in Figure 1. All the

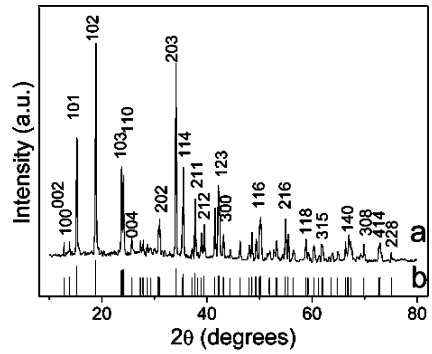

Figure 1. (a) Powered XRD pattern of the as-prepared CeHCF(II) and (b) standard XRD pattern of hexagonal CeHCF(II) (JCPDs card no. 83-2292).

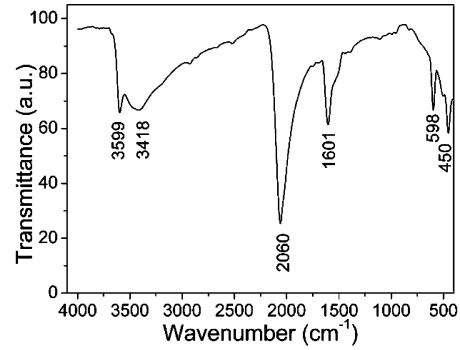

Figure 2. IR spectrum of the as-prepared CeHCF(II).

peaks of the as-prepared CeHCF(II) can be assigned to hexagonal symmetry of $KCe[Fe(CN)_6]\cdot 4H_2O$ (space group $P6_3/m$; $a = 7.392$ Å and $c = 13.87$ Å, JCPDS card no. 83-2292). No other peaks were observed, indicating high purity of the as-prepared samples. Compared to the standard XRD pattern, peaks (101), (102), and (203) show notably high intensity, indicating that the obtained $KCe[Fe(CN)_6]\cdot 4H_2O$ structures are preferentially oriented. This preferential orientation phenomenon was also observed in other reaction conditions. Longer deposition time and different depositing potentials will notably increase the intensity of peak (102) (see curves a, b, and c in Figure S1 in the Supporting Information). The relative intensity of peak (102) and (203) increases with the acidity of the electrolyte (see curves d, e, and f in Figure S1). When the molar rate of $Ce(NO_3)_3$ and $K_3[Fe(CN)_6]$ is 1:9, only the peaks (101) and (102) can be observed in the XRD pattern (curve h in Figure S1). This phenomenon suggests that the preferential orientation of $KCe[Fe(CN)_6]\cdot 4H_2O$ structures are under the influence of deposition parameters.

As PB and its analogues, there is a sharp asymmetric CN stretching vibration peak (ν(CN)) of ferrocyanide around 2060 cm^{-1} in the CeHCF(II) IR spectrum (Figure 2).[40] Two peaks appearing at 598 and 450 cm^{-1} correspond to the stretching mode of ν(MC) and bending mode of δ(MCN), respectively.[40] A broad band at around 3418 cm^{-1} and a sharp peak at 3599 cm^{-1} showed that there are two types of stretching vibrations of the O−H group, indicating that there are two types of H_2O in the structure. One is the interstitial water or zeolitic water, corresponding to the broad adsorptive band occurring at approximately 3418 cm^{-1}, which results from the association of water due to the H-bonding; this is similar to the case of PB.[41,42] The other is the water coordinated to Ce, corresponding to the peak at 3599 cm^{-1}. The peak at 1601 cm^{-1} is assigned to the bending vibrations of the O−H group in water. The IR spectrum of the as-prepared product shows that the CeHCF(II)

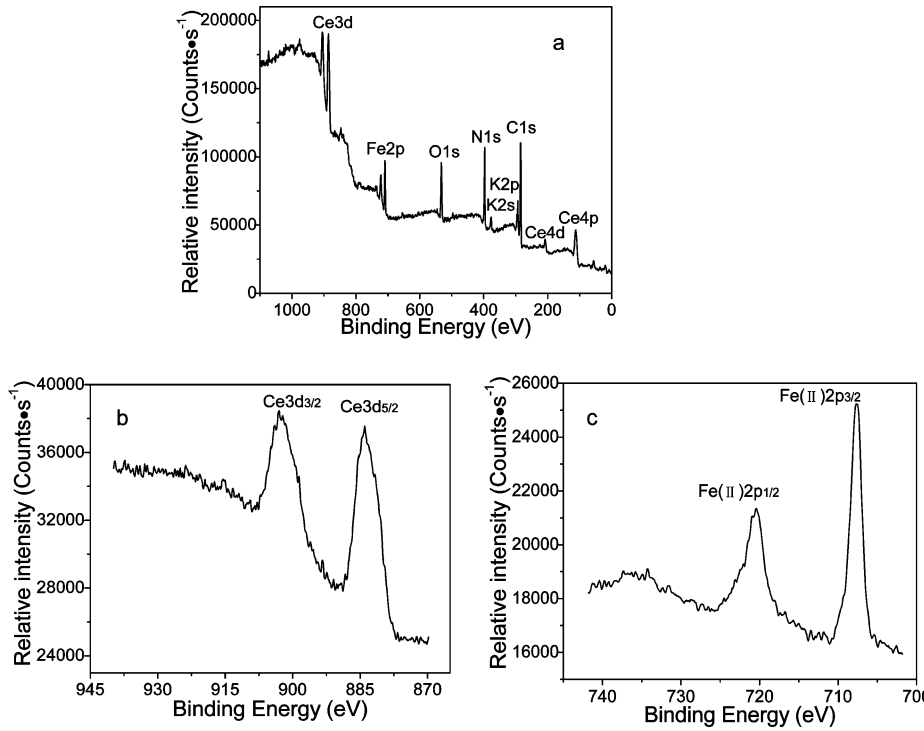

Figure 3. (a) Wide spectrum of the as-prepared CeHCF(II); (b) and (c) high-resolution spectra of Ce(3d) and Fe(2p), respectively.

is a metal hexacyanoferrate(II) compound with different types of crystal water.

Furthermore, the product was characterized by XPS for evaluating its composition and purity. Figure 3a shows the wide-scan XPS spectrum of CeHCF(II), in which the only detectable peaks observed are K, Ce, Fe, C, N, and O. The high-resolution XPS spectra of Ce(3d) and Fe(2p) are shown in Figure 3b and 3c, respectively. The two strong peaks taken for the Ce region at 884.0 and 902.0 eV are assigned to the Ce(3d) binding energy; the Fe(2p) peak appears at 707.0 and 720.0 eV. Some early XPS investigations on the electronic structures of Ce(3d) and Fe(2p) established very good standards for the studies of these prepared products. The Ce(3d) peaks are in good agreement with the reported spectra of trivalent cerium.[43] The measured binding energies of Fe(2p) are very close to the reported value of bivalent iron in other metal hexacyanoferrate(II) compounds, which are at about 708.0 and 722.0 eV;[44] there is no evidence of Fe(III) existing (the characteristic peak of Fe^{3+}(2p) is at 710.0 eV).[45] The peak areas of Ce(3d) and Fe(2p) are measured, and quantification of the peaks gives the atomic ratio of Ce:Fe to be approximately 1.12:1. It is approximate to the EDS result of 1.05:1 (Figure S2 in the Supporting Information). The molar ratio of Ce and Fe in XPS and EDS results support the XRD result that the as-prepared product is pure $KCe[Fe(CN)_6]\cdot 4H_2O$.

Figure 4 shows TG and DSC curves of the as-prepared CeHCF(II). In the TG curve, it is clear that a dehydration process starts at about 60 and ends at ~220 °C in three successive stages during which a percentage reduction in the sample mass by about 14.5% is observed. This value is close to the value 15.5% representing the relative molecular mass of the four water molecules to the molecular mass of $KCe[Fe(CN)_6]\cdot 4H_2O$. The DSC curve shows a structural variation indicated by three endothermic peaks observed at 103.6, 170.3, and 211.5 °C, respectively. This variation is due to the evolution of the four water molecules. The dehydration process in this manner is of special interest since it was observed in the IR investigations that the four water molecules in the crystal lattice of CeHCF(II)

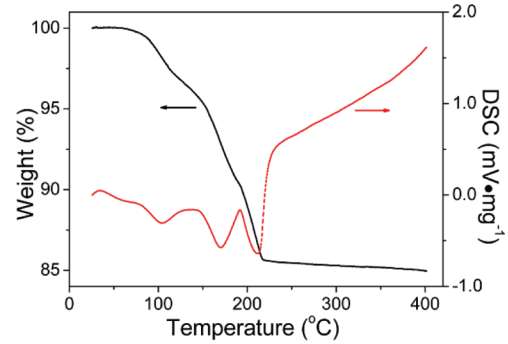

Figure 4. TG and DSC curves of the as-prepared CeHCF(II).

form two groups, and each group has its own peculiar character. This difference in character could be attributed to a difference in the chemical bonding between a certain water molecule and the crystal lattice because of its location in the network.

In the experiments, when an ITO electrode was placed in a solution with 5.0 mM $Ce(NO_3)_3$, 5.0 mM $K_3[Fe(CN)_6]$, and 0.1 M KNO_3 and was electrodeposited at −0.2 V for 500 s, microsized flowerlike and fusiform Christmas-tree-like products were observed, as shown in Figure 5. In a general view, there are plenty of flowerlike and fusiform Christmas-tree-like products, and the amount of flowerlike products is more than that of fusiform Christmas-tree-like ones. The magnified SEM images of individual flowerlike (Figure 5b) and fusiform Christmas-tree-like (Figure 5c) all have symmetrical dropwort structure, and the sizes are about 55−75 μm and 60−90 μm, respectively. Upon careful observation, all the products are shaped from individual hexagons with 1.2 μm side length and 0.5 μm thickness, as shown in Figure 5d.

The role of electrodepositing potential and time were also investigated in the preparation. When −0.2 V potential was applied, the size of as-prepared products increased with the deposition time (Figure S3 in the Supporting Information); if the deposited time was less than 500 s, the products showed

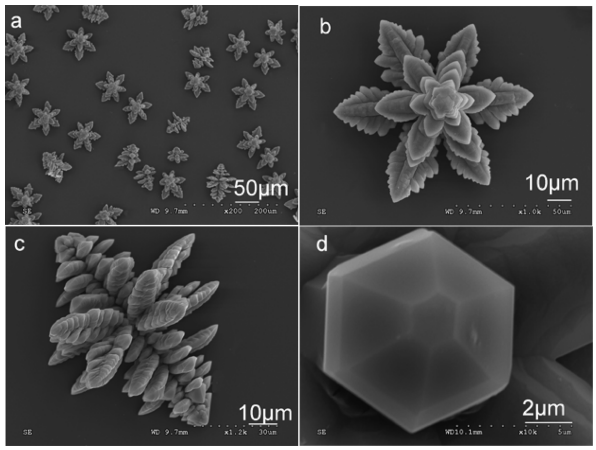

Figure 5. SEM images of CeHCF(II) microparticles deposited at −0.2 V for 500 s: (a) low magnitude, (b) individual flowerlike product, (c) individual fusiform Christmas-tree-like product, and (d) single hexagonal.

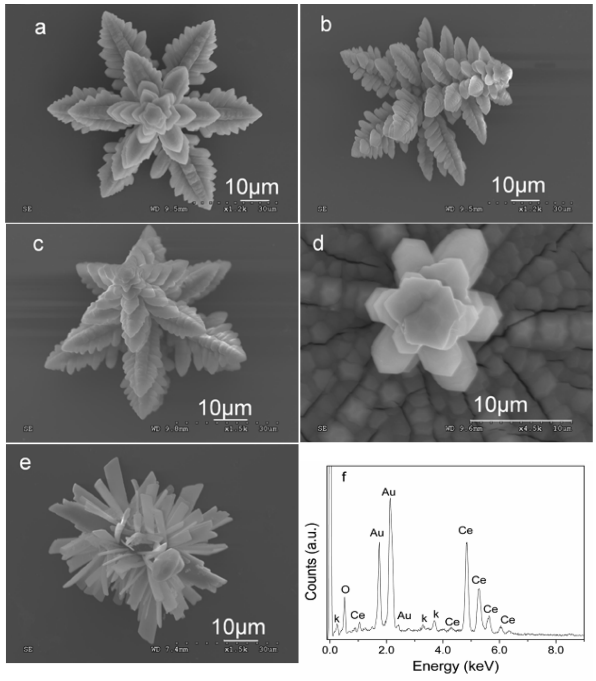

Figure 6. From (a) to (e) are SEM images of the CeHCF(II) flowerlike microproducts prepared at −0.4, −0.2, 0, 0.2, and 0.4 V; (f) is the EDS spectrum of the product prepared at 0.4 V.

poor symmetry (see Figure S3a, b in the Supporting Information). Longer deposition time such as 2000 s resulted in good symmetry and excellent crystallinity but reduced deposition layers (Figure S3d in the Supporting Information), which is caused by the preferential orientation of the products and in accord with the XRD results (curves a, b, and c in Figure S1). If the deposition time was kept changeless, well-crystallized products could be obtained when the depositing potential is under 0 V, and the sizes of each flowerlike product are almost equivalent (about 80 μm), as shown in Figure 6a−c. The products prefer a transverse growth rather than longitudinal at 0 V (Figure 6d). If the deposition potential was increased to 0.2 V, the products represent an aggregated zonal structure that is obviously different from that of under 0 V (Figure 6e); the EDS spectrum shown in Figure 6f proves a CeO_2 component. The above results indicated that the deposition potential and time played an important role in controlling the component and morphology of the electrodeposited CeHCF(II) microproducts.

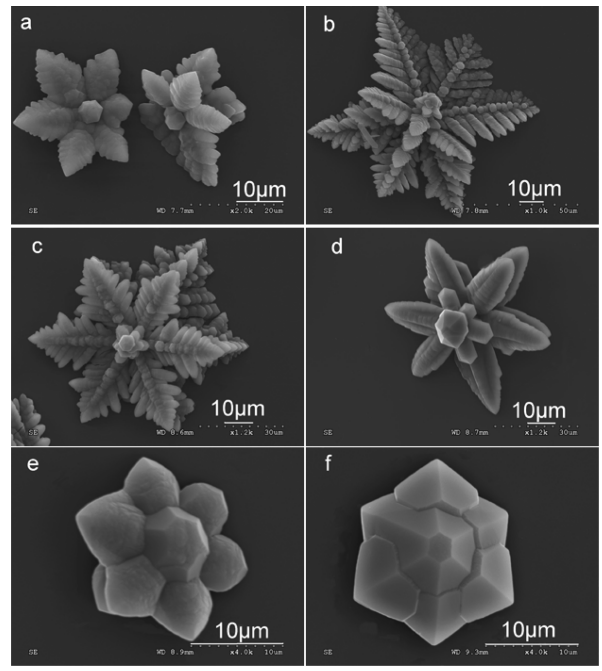

Figure 7. SEM images of the CeHCF(II) microparticles prepared at different molar ratios of Fe and Ce: (a) 1:9, (b) 1:4, (c) 1:2, (d) 2:1, (e) 4:1, and (f) 9:1.

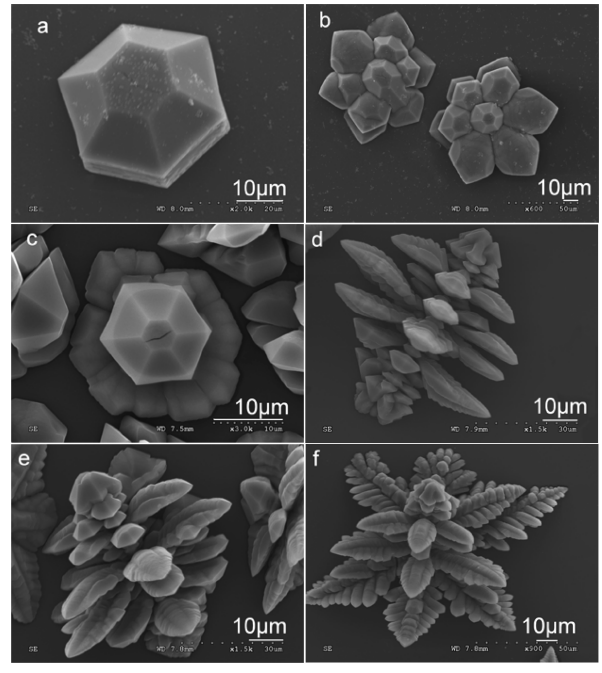

Figure 8. SEM images of the CeHCF(II) prepared at different pH values: (a) 1.0, (b) 2.0, (c) 3.0, (d) 4.0, (e) 5.0, and (f) 6.0.

SEM images in Figure 7 present the morphologies and microstructures of the crystals obtained upon altering the ratio of $Ce(NO_3)_3$ and $K_3[Fe(CN)_6]$. Keeping other parameters unchanged, when the molar ratios of $K_3[Fe(CN)_6]$ and $Ce(NO_3)_3$ are 1:9, 1:4, and 1:2, respectively, the size of flowerlike products increased from about 40 μm to ∼90 μm, as shown in Figure 7a, b, and c. If the concentration of $K_3[Fe(CN)_6]$ was bigger than $Ce(NO_3)_3$, the morphologies of flowerlike CeHCF(II) were slightly different from that of low-content $K_3[Fe(CN)_6]$ products; as shown in Figure 7d−f, the leaf of microflowers does not branch off, and the sizes are about 60, 20, and 20 μm corresponding the molar ratios 2:1, 4:1, and 9:1, respectively.

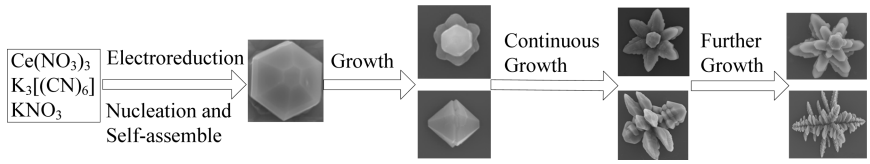

Figure 9. Schematic illustration of the formation process of flowerlike and fusiform Christmas-tree-like CeHCF(II) microparticles.

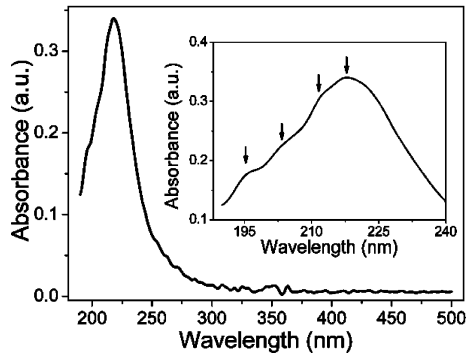

Figure 10. UV−vis absorption spectrum of the as-prepared CeHCF(II) microparticles. Inset is the amplified spectrum ranging from 190 to 280 nm.

Moreover, the layer of the microflowers is usually less than three in high content of $K_3[Fe(CN)_6]$ or $Ce(NO_3)_3$. Generally speaking, the structure variation and the layer number of CeHCF(II) can be adjusted through altering the content of $K_3[Fe(CN)_6]$ or $Ce(NO_3)_3$ in a moderate range.

In alkaline solutions, the strong interaction between metal ions and hydroxyl ions (OH^-) usually forms $M(OH)_x$; MHCFs are prepared only in acid media (pH < 7). The influence of solution acidity on the size and morphology of CeHCF(II) was also studied and shown in Figure 8. When the pH value of the electrolyte changed from 1.0 to 7.0, the size of the obtained products increased from 8.5 μm to about 100 μm, and the layer of the products altered from monolayer through double layer to multilayers correspondingly.

If $Ce(NO_3)_3$ was replaced by $(NH_4)_2Ce(NO_3)_6$, the as-prepared product showed cauliflower-like morphology (Figure S4a in the Supporting Information), and the molar ratio of Fe and N is about 1:6 in the EDS spectrum (Figure S4b in the Supporting Information), which means that there is no NH_4^+ ion in the products. Although the exact function of alkali ions and its analogues (such as NH_4^+ ion) in the formation of different CeHCF(II) shapes has not been clarified, it is undoubted that the morphology of CeHCF(II) is influenced by cations in electrolyte.

In order to exploit the formation mechanism of the as-prepared products, the cyclic voltammetric (CV) technique is also applied to study the deposition process of CeHCF(II). When the potential was scanned in the range of −0.5 to 1.0 V, a cathodic peak appeared at 0 V, which corresponds to the reduction of $[Fe(CN)_6]^{3-}$ to $[Fe(CN)_6]^{4-}$. The anodic peak corresponding to the oxidation of $[Fe(CN)_6]^{4-}$ to $[Fe(CN)_6]^{3-}$ appears at 0.3 V. The peak currents corresponding to the reaction of the $[Fe(CN)_6]^{3-/4-}$ redox couple decrease gradually with the increase of the scan cycles (see Figure S5 in the Supporting Information), which indicates the formation of CeHCF(II) on the electrode surface. On the basis of experimental results mentioned above, a possible formation mechanism for the flowerlike and fusiform Christmas-tree-like CeHCF(II) microparticles might be proposed as shown in Figure 9. First, when designed potential was applied to the ITO electrode, $Fe(CN)_6^{3-}$ was reduced to $Fe(CN)_6^{4-}$ at the electrode/electrolyte interface, and a chemical reaction to form plenty of tiny CeHCF(II) nuclei and nucleation of primary particles occurred on the electrode surface:

$$Fe(CN)_6^{4-} + Ce^{3+} + K^+ + 4H_2O \rightarrow KCe[Fe(CN)_6]\cdot 4H_2O \quad (1)$$

Accompanying the continuous formation, these primary particles self-assembled into hexagonal structures (Figure 5d) by controlled growth of the cumulated species on the existing nuclei, and then the hexagonal structure directionally grew along the C_6 and three C_2 axes. Double-layered flowerlike and fusiform-like products are formed in the early growing period. The products layer increases with the deposition time, and at last, the flowerlike (Figure 5b) and fusiform Christmas-tree-like products (Figure 5c) were formed. When the C_6 axis is perpendicular to the electrode surface, the initial hexagonal lies on the electrode surface, flowerlike products can be developed, and fusiform Christmas-tree-like microparticles correspond to the C_6 axis parallel to the electrode surface. The hexagonal structures are stochastic on the electrode surface. Because the prostrate hexagonal is more stable than the vertical one, flowerlike CeHCF(II) products exceed fusiform Christmas-tree-like microparticles, which can be seen in Figure 5a. Different cations may lead to the growth of small crystals in different ways and finally result in different shapes; however, the growth mechanism of different cations should be further investigated.

The absorption spectrum of the as-prepared microsized CeHCF(II) in the UV−vis region is shown in Figure 10. As a result of the f−d electron transitions, CeHCF(II) intensively absorbs UV light in the range from 190 to 280 nm, and the magnified spectrum (inset in Figure 10) shows four peaks appearing at 195.5, 203.6, 211.7, and 217.7 nm, respectively, which is in agreement with the literature.[46] Compared with the results of above literature, the absorption peaks of Ce^{3+} shift to higher energy. This different spectral behavior may be attributed to the different crystal field interactions caused by ligands banded to Ce^{3+}. In CeHCF(II), the crystal field splitting energy caused by CN^- ions is higher than that of F^-, PO_4^{3-}, and $P_2O_7^{3-}$, which would result in a higher energy needed d−f transition and a blue shift in the CeHCF(II) absorption spectrum.

The excitation spectrum of the as-prepared CeHCF(II) products monitored at the emission wavelength of 350 nm is shown in Figure 11a. It has a broad band ranging from 228 to 276 nm peaking at 250 nm and a minor shoulder emerging at about 238 nm. To simplify the discussion, we used two bands to fit the excitation curve with a Gaussian distribution. It is clear that the fitted broad band shows two Gaussian peaks with maximum appearing at 236 and 250 nm (the green lines in Figure 11a), which correspond to the transitions from the ground state $^2F_{5/2}$ of Ce^{3+} to the excited Ce^{3+} 5d states split by the crystal field. However, the intensity ratio of these two peaks is about 13.5, i.e., the intensity of the peak at 236 nm is very little and can be neglected. This phenomenon may be contributed to the high crystal field splitting energy caused by CN^- bonding to Ce^{3+}. Upon excitation at 250 nm, CeHCF(II) exhibits a strong

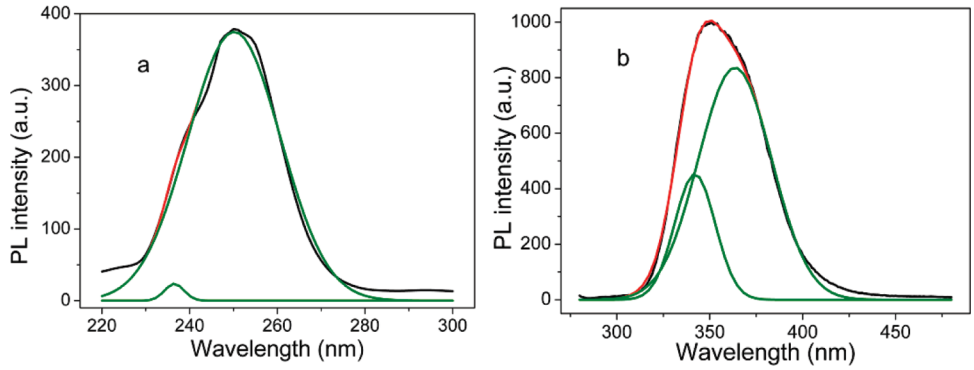

Figure 11. Excitation (a) and emission (b) spectra of the as-prepared CeHCF(II) microparticles. Black line is the original sampling spectrum, red line is the fitting curve, and green lines are the simulated Gauassian curves of Ce^{3+}.

ultraviolet emission peak centered at 350 nm, as shown in Figure 11b. The emission of Ce^{3+} could be fitted with two broad bands with maximal peaks at 341 and 363 nm, respectively, which are assigned to the $5d-{}^2F_{5/2}$ and $5d-{}^2F_{7/2}$ transitions due to spin orbit splitting of the $4f^1$ ground state of Ce^{3+}.[16,21] The PL properties of different shapes of CeHCF(II) also have been investigated. When the products are prepared at different molar rates of $Ce(NO_3)_3$ and $K_3[Fe(CN)_6]$, there is no obvious difference in the excitation and emission spectra (see Figure S6 in the Supporting Information). In order to compare the PL properties of the as-prepared CeHCF(II), micron-sized luminescent $CePO_4$ synthesized through simple chemical method is chosen as reference (see Figure S7 in the Supporting Information). In the excitation spectrum of $CePO_4$, the two simulated Gaussian peaks are at 256 and 317 nm, and the intensity ratio is about 5.0, which indicates the crystal field splitting energy in $CePO_4$ is less than that of CeHCF(II). Upon excitation at 271 nm, $CePO_4$ also exhibits strong ultraviolet emission peaks centered at 350 nm (Figure S7b in the Supporting Information). The PL intensity ratio of CeHCF(II) and $CePO_4$ with equivalent concentration is about 1.0:0.7 at 350 nm. The enhanced ultraviolet emission of the as-prepared CeHCF(II) microparticles may be rooted in two aspects, one is the flowerlike and fusiform Christmas-tree-like microsized products, and the other is the proper distance of Ce^{3+} ions in CeHCF(II). These results indicate that the luminescent properties of the microstructured CeHCF(II) are largely affected by factors such as the morphology, the particle size, and the bonding ligands.

Conclusions

In summary, flowerlike and fusiform Christmas-tree-like CeHCF(II) microparticles have been synthesized by a facile electrochemical deposition method. The prepared sample is a stoichiometric compound of $KCe[Fe(CN)_6]\cdot 4H_2O$. It is found that the size and morphology of flowerlike and fusiform Christmas-tree-like CeHCF(II) microparticles were altered by electrodepositing potential and time, the molar ratio of $Ce(NO_3)_3$ and $K_3[Fe(CN)_6]$, and the acidity of electrolyte. The formation mechanism of the flowerlike and fusiform Christmas-tree-like structure has been investigated, and the directional growth along the C_6 and three C_2 axes of the self-assembled hexagonal structures clearly contributes to the creation of such a structure. Room-temperature UV−vis absorption and PL properties of CeHCF(II) have also been investigated. The obtained samples showed good ultraviolet luminescent properties, which could be related to their different morphologies, particle sizes, and bonding ligands. The enhanced PL properties of microsized CeHCF(II) may open up new applications in the assembly of microscale ultraviolet optical devices.

Acknowledgment. We greatly appreciate the support of the National Natural Science Foundation of China for the Key Program (20635020), Creative Research Group (20821063). L.-D.F. also thanks the Postdoctoral Program of Jiangsu Province (0701013C) and the Natural Science Foundation of the Jiangsu Higher Education Institutions of China (Grant 07KJD150016) for support. J.-J.Z. thanks the support of open foundation from State Key Laboratory of Bioelectronics (Chien-Shiung Wu) Laboratory.

Supporting Information Available: XRD pattern, EDS spectra, and SEM images of the CeHCF(II) prepared at other experimental factors, PL spectra of of microsized $CePO_4$, and different molar rate of $Ce(NO_3)_3$ and $K_3[Fe(CN)_6]$. The material is available free of charge via the Internet at http://pubs.acs.org.

References and Notes

(1) (a) van Loaf, E. V. D.; Dorenbos, P.; Van Eijk, C. W. E.; Kramer, K.; Guide, H. U. *Appl. Phys. Lett.* **2000**, *77*, 1467. (b) van Loef, E. V. D.; Dorenbos, P.; Van Eijk, C. W. E.; Krämer, K.; Güdel, H. U. *Appl. Phys. Lett.* **2001**, *79*, 1573. (c) Parker, D.; Dickins, R. S.; Puschmann, H.; Crossland, C.; Howard, J. A. K. *Chem. Rev.* **2002**, *102*, 1977. (d) Vogler, A.; Kunkely, H. *Inorg. Chim. Acta* **2006**, *59*, 4130.

(2) (a) Kido, J.; Okamoto, Y. *Chem. Rev.* **2002**, *102*, 2357. (b) Zhang, J.; Badger, P. D.; Geib, Petoud, S. J. S. *Angew. Chem., Int. Ed.* **2005**, *44*, 2508. (c) Liu, J.; Li, Y. *Adv. Mater.* **2007**, *19*, 1118.

(3) (a) Cha, A.; Snyder, G. E.; Selvin, P. R.; Bezanilla, F. *Nature (London)* **1999**, *402*, 809. (b) Motson, G. R.; Fleming, J. S.; Brooker, S. *Adv. Inorg. Chem.* **2004**, *55*, 361. (c) Yuan, J.; Wang, G. *Trac Trends Anal. Chem.* **2006**, *25*, 490.

(4) (a) Montalti, M.; Prodi, L.; Zaccheroni, N.; CharbonniMre, L.; Douce, L.; Ziessel, R. *J. Am. Chem. Soc.* **2001**, *123*, 12694. (b) HemmilS, I.; Laitala, V. *J. Fluoresc.* **2005**, *15*, 529.

(5) (a) Schlotter, P.; Schmidt, R.; Schneider, J. *Appl. Phys. A* **1997**, *64*, 417. (b) Riwotzki, K.; Meyssamy, H.; Schnablegger, H.; Kornowski, A.; Markus, H. *Angew. Chem., Int. Ed.* **2001**, *40*, 573. (c) Nikl, M.; Mihokova, E.; Malkova, Z.; Vedda, A.; Martini, M.; Shimmamura, K.; Sukuda, T. *Phys. Rev. B* **2002**, *66*, 184101.

(6) (a) Blasse, G.; Grabmaier, B. C. *Luminescent Materials*; Springer-Verlag: Berlin, 1994. (b) Dorenbos, P.; Pierron, L.; Dinca, L.; Van Eijk, C. W. E.; Kahn-Harari, A.; Viana, B. *J. Phys.: Condens. Matter* **2003**, *15*, 511.

(7) (a) Zanella, G.; Zannoni, R.; Dall'Igna, R.; Locardi, B.; Polato, P.; Bettinelli, M.; Marigo, A. *Nucl. Instrum. Methods Phys. Res., Sect. A* **1994**, *345*, 198. (b) Okada, F.; Togata, S.; Otho, K.; Koda, S. *J. Appl. Phys.* **1994**, *75*, 49. (c) Martini, M.; Meinardi, F.; Vedda, A.; Dafinei, I.; Lecoq, P.; Nikl, M. *Nucl. Instrum. Methods Phys. Res., Sect. B* **1996**, *116*, 116. (d) Kucuk, A.; Clare, A. G. *Opt. Mater.* **1999**, *13*, 279. (e) Baccaro, S.; Dall'Igna, R.; Fabeni, P.; Martini, M.; Mares, J. A.; Meinardi, F.; Nikl, M.; Nitsch, K.; Pazzi, G. P.; Polato, P.; Vedda, A.; Zanella, G.; Zannoni, R. *J. Lumin.* **2000**, *87*, 673. (f) Nikl, M.; Nitsch, K.; Mihokova, E.; Solovieva, N.; Mares, J. A.; Fabeni, P.; Pazzi, G. P.; Martini, M.; Vedda, A.; Baccaro, S. *Appl. Phys. Lett.* **2000**, *77*, 2159. (g) La Roche, M.; Girard, S.; Moncorge, R.; Bettinelli, M.; Abdulsabirov, R.; Semashko, V. *Opt. Mater.* **2003**, *22*, 147. (h) Murata, T.; Sato, M.; Yoshida, H.; Morinaga, K. *J. Non-Cryst. Solids* **2005**, *351*, 312.

(8) Auzel, F.; Goldner, P. *Opt. Mater.* **2001**, *16*, 93.

(9) Sun, R.; Wang, Y.; Wang, D.; Zheng, Q.; Kyllo, E. M.; Gustafson, T. L.; Epstein, A. J. *Appl. Phys. Lett.* **2000**, *76*, 634.
(10) Justicia, I.; Ordejón, P.; Canto, G.; Mozos, J. L.; Fraxedas, J.; Battiston, G. A.; Gerbasi, R.; Figueras, A. *Adv. Mater.* **2002**, *14*, 1399.
(11) Chikan, V.; Kelley, D. F. *Nano Lett.* **2002**, *2*, 141.
(12) Wuister, S. F.; Swart, I.; Driel, F.; Hickey, S. G.; Donegá, C. M. *Nano Lett.* **2003**, *3*, 503.
(13) Wang, Z. *Adv. Mater.* **2003**, *15*, 432.
(14) Wang, X.; Song, J.; Liu, J.; Wang, Z. *Science* **2007**, *316*, 102.
(15) Alberti, G.; Constantino, U. *J. Mol. Catal.* **1984**, *27*, 235.
(16) Tang, C.; Bando, Y.; Golberg, D.; Ma, R. *Angew. Chem., Int. Ed.* **2005**, *44*, 576.
(17) Kömpe, K.; Lehmann, O.; Haase, M. *Chem. Mater.* **2006**, *18*, 4442.
(18) Ma, L.; Chen, W.; Zheng, Y.; Xu, Z. *Mater. Res. Bull.* **2008**, *43*, 2840.
(19) Bu, W.; Hua, Z.; Chen, H.; Shi, J. *J. Phys. Chem. B* **2005**, *109*, 14461.
(20) Li, G.; Chao, K.; Peng, H.; Chen, K.; Zhang, Z. *J. Phys. Chem. C* **2008**, *112*, 16452.
(21) Bu, W.; Hua, Z.; Chen, H.; Zhang, L.; Shi, J. *Chem. Lett.* **2004**, *33*, 312.
(22) Luo, F.; Jia, C.-J.; Song, W.; You, L.-P.; Yan, C.-H. *Cryst. Growth Des.* **2005**, *5*, 137.
(23) Liu, J. F.; Yao, Q. H.; Li, Y. D. *Appl. Phys. Lett.* **2006**, *88*, 173119.
(24) Liu, J. F.; Li, Y. D. *Adv. Mater.* **2007**, *19*, 1118–1122.
(25) Deng, H.; Yang, S.; Xiao, S.; Gong, H.-M.; Wang, Q.-Q. *J. Am. Chem. Soc.* **2008**, *130*, 2032.
(26) Moses, W. W.; Derenzo, S. E. *Nucl. Instrum. Methods A* **1990**, *299*, 51.
(27) Shimamura, K.; Vìllora, E. G.; Nakakita, S.; Nikl, M.; Ichinose, N. *J. Cryst. Growth* **2004**, *264*, 208.
(28) Zhu, L.; Li, Q.; Liu, X.; Li, J.; Zhang, Y.; Meng, J.; Cao, X. *J. Phys. Chem. C* **2007**, *111*, 5898.
(29) Kasuya, R.; Isobe, T.; Kuma, H.; Katano, J. *J. Phys. Chem. B* **2005**, *109*, 22126.
(30) Li, Q.; Yam, V. W.-W. *Angew. Chem., Int. Ed.* **2007**, *46*, 3486.
(31) Liang, H.; Tao, Y.; Zeng, Q.; He, H.; Wang, S.; Hou, X.; Wang, W.; Su, Q. *Mater. Res. Bull.* **2003**, *38*, 797.
(32) Chiodini, N.; Fasoli, M.; Martini, M.; Rosetta, E.; Spinolo, G.; Vedda, A.; Nikl, M.; Solovieva, N.; Baraldi, A.; Capelletti, R. *Appl. Phys. Lett.* **2002**, *81*, 4374.
(33) Baraldi, A.; Capelletti, R.; Chiodini, N.; Mora, C.; Scotti, R.; Uccellini, E.; Vedda, A. *Nucl. Instrum. Methods Phys. Res., Sect. A* **2002**, *486*, 408.
(34) Vedda, A.; Baraldi, A.; Canevali, C.; Capelletti, R.; Chiodini, N.; Francini, R.; Martini, M.; Morazzoni, F.; Nikl, M.; Scotti, R.; Spinolo, G. *Nucl. Instrum. Methods Phys. Res., Sect. A* **2002**, *486*, 259.
(35) Vedda, A.; Chiodini, N.; Di Martino, D.; Fasoli, M.; Martini, M.; Moretti, F.; Rosetta, E.; Spinolo, G.; Nikl, M.; Solovieva, N.; Baraldi, A.; Capelletti, R. *J. Non-Cryst. Solids* **2004**, *345 & 346*, 338.
(36) Vedda, A.; Chiodini, N.; Di Martino, D.; Fasoli, M.; Griguta, L.; Moretti, F.; Rosetta, E. *J. Non-Cryst. Solids* **2005**, *351*, 3699.
(37) Vedda, A.; Chiodini, N.; Di Martino, D.; Fasoli, M.; Morazzoni, F.; Moretti, F.; Scotti, R.; Spinolo, G.; Baraldi, A.; Capelletti, R.; Mazzera, M.; Nikl, M. *Chem. Mater.* **2006**, *18*, 6178.
(38) (a) Assefa, Z.; Shankle, G.; Patterson, H. H.; Reynolds, R. *Inorg. Chem.* **1994**, *33*, 2187. (b) Assefa, Z.; Patterson, H. H. *Inorg. Chem.* **1994**, *33*, 6194. (c) Omary, M. A.; Webb, T. R.; Assefa, Z.; Shankle, G. E.; Patterson, H. H. *Inorg. Chem.* **1998**, *37*, 1380. (d) Omary, M. A.; Patterson, H. H. *Inorg. Chem.* **1998**, *37*, 1060. (e) Rawashdeh-Omary, M. A.; Larochelle, C. L.; Patterson, H. H. *Inorg. Chem.* **2000**, *39*, 4527.
(39) (a) Kaneko, M.; Takabayashi, N.; Yamauchi, Y.; Yamada, A. *Bull. Chem. Soc. Jpn.* **1984**, *57*, 156. (b) Kaneko, M.; Hou, X.-H.; Yamada, A. *J. Chem. Soc., Faraday Trans. 1* **1986**, *82*, 1637. (c) Feng, L. D.; Shen, J. M.; Li, X. H.; Zhu, J. J. *J. Phys. Chem. C* **2008**, *112*, 7617.
(40) Nakamoto, K. *Infrared and Raman Spectra of Inorganic and Coordination Compounds*; John Wiley & Sons, Inc.: New York, 1986.
(41) Wilde, R. E.; Ghosh, S. N.; Marshall, B. J. *Inorg. Chem.* **1970**, *9*, 2522.
(42) Itaya, K.; Uchida, I.; Neff, V. D. *Acc. Chem. Res.* **1986**, *19*, 162.
(43) (a) Yusaku, T.; Xia, Q.; Akihide, T.; Hiroyasu, N.; Katsutoshi, N. *Appl. Catal., A* **2005**, *296*, 63. (b) Wang, X. M.; Zeng, X. Q.; Wu, G. S.; Yao, S. S.; Lai, Y. J. *J. Alloys Compd.* **2008**, *456*, 384. (c) Bach, H. T.; Venhaus, T. J.; Paglieri, S. N.; Oona, H.; Allen, T. H.; Schwarz, R. B.; Wermer, J. R. *J. Alloys Compd.* **2007**, *446−447*, 567. (d) Xiao, W. D.; Guo, Q. L.; Wang, E. G. *J. Phys. Chem. B* **2005**, *109*, 4953.
(44) (a) Sauter, S.; Wittstock, G.; Szargan, R. *Phys. Chem. Chem. Phys.* **2001**, *3*, 562. (b) Cui, X. P.; Hong, L.; Lin, X. Q. *J. Electroanal. Chem.* **2002**, *526*, 115. (c) Wu, P.; Cai, C. X. *J. Solid State Chem.* **2004**, *8*, 538. (d) Malik, M. A.; Kulesza, P. J.; Wlodarczyk, R.; Wittstock, G.; Szargan, R.; Bala, H.; Galus, Z. *Electroanalysis* **2005**, *9*, 403. (e) Wu, P.; Cai, C. X. *J. Solid State Chem.* **2005**, *17*, 1583. (f) Yang, G. C.; Shen, Y.; Wang, M. K.; Chen, H. J.; Liu, B. F.; Dong, S. J. *Talanta* **2006**, *68*, 741. (g) Wu, P.; Shi, Y. M.; Cai, C. X. *J. Solid State Chem.* **2006**, *10*, 270. (h) Agnihotry, S. A.; Singh, P.; Joshi, A. G.; Singh, D. P.; Sood, K. N.; Shivaprasad, S. M. *Eletrochim. Acta* **2006**, *51*, 4291.
(45) Mullica, D. F.; Perkins, H. O.; Sappenfield, E. L. *Inorg. Chim. Acta* **1988**, *142*, 9.
(46) (a) Heaps, W. S.; Elias, L. R.; Yen, W. M. *Phys. Rev. B* **1976**, *13*, 94. (b) Wojtowicz, A. J.; Balcerzyk, M.; Berman, E.; Lempicki, A. *Phys. Rev. B* **1994**, *49*, 14880. (c) Fang, Y. P.; Xu, A. W.; Song, R. Q.; Zhang, H. X.; You, L. P.; Yu, J. C.; Liu, H. Q. *J. Am. Chem. Soc.* **2003**, *125*, 16025. (d) Wang, Z. L.; Quan, Z. W.; Jia, P. Y.; Lin, C. K.; Luo, Y.; Chen, Y.; Fang, J.; Zhou, W.; O'Connor, C. J.; Lin, J. *Chem. Mater.* **2006**, *18*, 2030. (e) Zhu, L.; Li, Q.; Liu, X.; Li, J.; Zhang, Y.; Meng, J.; Cao, X. *J. Phys. Chem. C* **2007**, *111*, 5898.

JP900925P